http://journal.uir.ac.id/index.php/JGEET

E-ISSN : 2541-5794
P-ISSN : 2503-216X

Journal of Geoscience,
Engineering, Environment, and Technology
Vol xx No xx 20xx

RESEARCH ARTICLE

Estimation of Subsurface Structure Using Euler Deconvolution and SVD Methods of Geomagnetic Data in the Non-Volcanic Geothermal Area of Tahi Ite Village, Bombana, Southeast Sulawesi, Indonesia

Rani Chahyani[1,*], Abdul Manan[2]

[1] *Study Program of Physical Education, Institut Agama Islam Negeri (IAIN) Kendari, Kendari City, Indonesia*
[2] *Department of Geophysical Engineering, Universitas Halu Oleo, Kampus Hijau Bumi Tridharma, Kendari City, Indonesia*

* Corresponding author : rani.chahyani@gmail.com
Tel.:+62-822-4075-0000
Received: Oct 1, 2016; Accepted: Nov 20, 2016.
DOI: 10.24273/jgeet.2016.1.2.001

Abstract

This study aims to estimate the presence of subsurface structures in the geothermal area of Tahi Ite Village, Bombana Regency, Southeast Sulawesi by using geomagnetic data collected in the field at 656 measurement points using a PPM unit divided into nine survey lines oriented N0°S, with distances between measurement points and between survey lines of approximately 50 m and 180 m, respectively. Based on the research results, the Total Magnetic Intensity (TMI) values for the study area ranged from 42,375.605 to 42,817.045 nT. A value range of 441.44 nT indicates the presence of rock magnetic heterogeneity in the geothermal manifestation area. After applying Diurnal Correction and IGRF Correction, the Total Magnetic Anomaly (TMA) values were found to be approximately -136.89 to 200 nT. The Local Magnetic Anomaly (LMA) was obtained after performing an upward continuation process through four continuation stages up to an altitude of 1,700 m from the reference surface, The Local Magnetic Anomaly (LMA) was obtained after performing an upward continuation process through four continuation stages up to a height of 1,700 m from the reference surface, and was found to be within a range of approximately -120 to 60 nT. Subsequently, Reduced to the Pole (RTP) processing was applied to transform the magnetic response so that it lies above its causative source and exhibits a monopolar nature. On the RTP results, the Euler Deconvolution (DE) method with a Structural Index of N=0 and the Second Vertical Derivative (SVD) method were applied to infer the presence of subsurface structures. The results show the presence of magnetic anomaly patterns suggesting strong structural control with a dominant North–South orientation. It is estimated that there are approximately five to nine minor faults with depths ranging from <15 m (Very Shallow) to >55 m (Deep), and it is known that approximately two minor faults intersect the Tahi Ite hot spring. The existence of these minor faults is thought to act as thermal conduction pathways and channels for the migration of hydrothermal fluids to the surface with the water source in the reservoir originating from surface or meteoric water. These findings are also supported by the presence of outcrops, further confirming that the Tahi Ite Village geothermal system is non-volcanic in nature and controlled by secondary structures in the form of minor faults.

Keywords: Tahi Ite Village, Geomagnetic data, Residual magnetic anomaly, DE method, SVD method, Minor faults.

1. Introduction

Global energy consumption continues to rise in line with population growth and increasing industrialization (Yan et al., 2024; Akyol, 2022). Meanwhile, oil and gas reserves are dwindling. Therefore, other potential energy sources are needed to be developed as sustainable and environmentally friendly alternatives. Geothermal energy is a promising solution due to its relative safety and significant potential (Huang et al., 2023; Jamil et al., 2023; Dashti and Korzani, 2021). This energy source produces relatively low greenhouse gas emissions and is capable of providing stable baseload power (Ricks et al., 2025; Gutiérrez-Negrín, 2024; Aljubran and Horne, 2024; IRENA and IGA, 2023; Titus et al., 2023; Manzella, 2017).

Indonesia is one of the countries in the world with geothermal potential as an energy source (Taufan et al., 2020; Manyoe and Hutagalung, 2020). This is because it is tectonically located at the intersection of three major world plates, namely the Eurasian, Indo-Australian, and Pacific plates. The meeting of these three plates has created unique geological conditions for the formation of geothermal systems in Indonesia (Massinai et al., 2026; Saepuloh et al., 2026; Kusnadi, 2021; Alpine et al., 2022). Data from the Ministry of Energy and Mineral Resources (ESDM) in 2018 shows that Indonesia's geothermal potential is approximately 11,073 MW, with approximately 17,506 MW of reserves. These geothermal sources are distributed across 331 different locations from Sabang to Merauke (https://www.esdm.go.id/).

Geothermal systems in Indonesia are generally formed in volcanic environments, but there are a number of geothermal manifestations in non-volcanic environments, particularly on the island of Sulawesi, with 60 locations recorded as of 2015 by the Geological Agency (Risdianto et al., 2015; https://www.iagi.or.id/). Volcanic systems are closely related to volcanic activity, while non-volcanic systems are associated with the presence of subsurface fault zones that act as conduits for the circulation of heat and hydrothermal fluids (Annuar et al., 2021; Stober and Bucher, 2021). In Southeast Sulawesi, geothermal manifestations typically appear in sedimentary and metamorphic rocks (Hermawan et al., 2011). This situation suggests a strong structural control on the formation of geothermal systems, rather than a direct magmatic heat source (Annuar et al., 2021; Stober and Bucher, 2021). Among the geothermal potential areas in Southeast Sulawesi is Tahi Ite Village, Rarowatu District, Bombana Regency, characterized by the presence of hot springs. This manifestation indicates an active geothermal system, but knowledge of the subsurface structures that control thermal conduction and geothermal fluid migration in this area remains limited. However, understanding the subsurface structures, particularly lithological contacts and

fault zones, is crucial for assessing geothermal resources and evaluating potential geological hazards associated with active faults (Annuar et al., 2021; Castellano et al., 2021; Chen et al., 2024). The Tahi Ite hot springs generally taste brackish with a relatively low temperature, and are known by the local community as a tourist attraction.

One of the geophysical methods that has proven reliable in conducting geothermal exploration is the geomagnetic method. This method is widely used because of its sensitivity to variations in rock magnetization, which is generally reduced in zones experiencing hydrothermal alteration (Thilakarathna et al., 2025; Pandarinath et al., 2023; Pandarinath et al. 2019). Geomagnetic data in the form of variations in Total Magnetic Intensity is obtained through measurements above the Earth's surface using a Magnetometer. In its implementation, data processing employs the Euler Deconvolution (DE) method as this method has proven effective in characterizing subsurface structures, particularly geothermal pathways controlled by fault zones, estimating the lateral location and depth of anomalous sources (Ghanbarifar et al., 2024a; Ghanbarifar et al., 2024b; Pham et al., 2024). Meanwhile, the and Second Vertical Derivative (SVD) method is used to determine and clarify the edges and positions of the subsurface anomaly source, and has also proven to be effective (Ming et al., 2021).

This research reveals the existence of subsurface structures, particularly minor faults that control thermal activity at hot springs in the research area (manifestation area), and is urgently to be carried out as it relates to the Indonesian government's plan to diversify energy resources through the development of new, renewable, and environmentally friendly energy, commonly known as Green Energy. It is hoped that geothermal energy can become a potential energy resource for development on the island of Sulawesi.

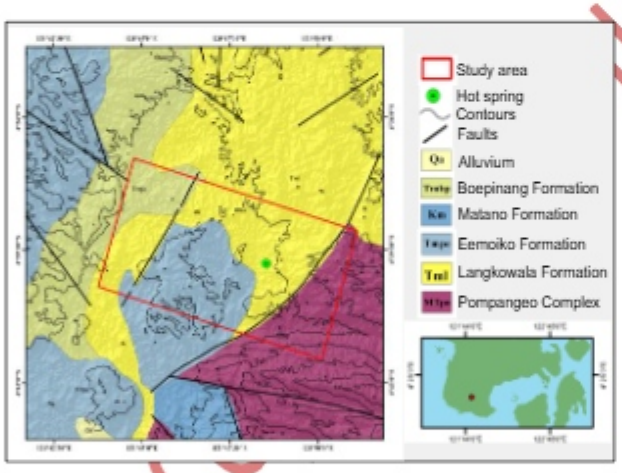

Fig 1. Distribution map of rock formations in Tahi Ite Village (modified from Simandjuntak et al. (1993)).

2. Geological Setting

The Tahi Ite geothermal manifestation is located in Rarowatu District, Bombana Regency, Southeast Sulawesi, and belongs to a non-volcanic geothermal system primarily controlled by geological structures in the form of regional and local fault networks. The geology of this region is composed of sedimentary rock units, metamorphic complexes, and Quaternary-aged alluvial deposits, which record the complex dynamics of Southeast Sulawesi's tectonic evolution (Simandjuntak et al., 1993; Surono, 2013). Sedimentary units in this area are dominated by sandstone, mudstone, conglomerate, and limestone, formed in shallow marine to coastal depositional environments. Meanwhile, metamorphic rocks encountered include schist, gneiss, quartzite, and amphibolite, formed by metamorphism under high pressure and temperature conditions. These various lithological units are intersected by fault systems that play a significant role in controlling the flow and circulation of subsurface fluids. The occurrence of geothermal manifestations in the form of hot springs scattered along fault lines that cut through sedimentary and metamorphic rocks indicates a strong structural control influence on geothermal fluid movement. Therefore, this system is not directly related to volcanic activity but rather is controlled by local geological structural conditions (Hermawan et al., 2011; Annuar et al., 2021; Stober and Bucher, 2021). Figure 1 displays the distribution map of rock formations in Tahi Ite Village, which serve as the primary geological framework controlling the occurrence of geothermal manifestations at the study site. In general, the rock formations found are the Langkowala Formation, the Eemoiko Formation, and the Pompangeo Complex.

3. Research Method

3.1 Study Area

This research was conducted in Tahi Ite Village, Rarowatu District, Bombana Regency, Southeast Sulawesi, Indonesia. Geothermal manifestations in this area are in the form of hot springs that emerge on the surface through sedimentary and metamorphic rocks, and are a non-volcanic geothermal system (Risdianto et al., 2015). Geographically, this area is located at approximately 4°36 ′–4°38 ′ S latitude and 121°52 ′–121°54 ′ E longitude.

3.2 Geomagnetic Data Acquisition

Geomagnetic data were obtained through direct field measurements at 656 measurement points with N0°S orientation using 1 unit of GPM-10 Proton Magnetometer. The measurement points were spread across 9 lines with a distance of approximately 50 m between measurement points and 180 m between lines. To ensure the accuracy of the coordinates of the measurement points, GPS was also used, in addition to being recorded automatically on the Magnetometer unit. The measured geomagnetic data was in the form of total magnetic intensity (TMI) values. Measurements were carried out 4 times in repetition to minimize interference and unnecessary short-period magnetic fluctuations. The TMI, which represents each measurement point, was determined based on the Mean or Median value of the 4 repetitions. All measurement data was stored digitally on the Magnetometer unit, and was also recorded manually on logsheets as part of data security and quality control.

3.3 Data Processing

Geomagnetic data processing was carried out to obtain magnetic anomalies, especially residual anomalies that describe local conditions in the subsurface of the research area, especially the presence of geological structures that play a role in the local geothermal system. These geological structures are mainly in the form of fault zones. Data processing procedures follow the geomagnetic data processing standards commonly applied in geothermal and structural exploration, including data quality control, geomagnetic data reduction in the form of diurnal correction and IGRF correction, Upward Continuation, determination of residual anomalies, and Reduction to the Pole (RTP), Euler Deconvolution and Second Vertical Derivative (SVD) analysis.

3.4 Data Quality Control

Prior to data processing, the quality of the measurement data must be ensured. Data quality control is performed to eliminate cultural noise, instrument instability, or localized disturbances. If measurement results show abnormal deviations

from surrounding data points, an evaluation is performed to ensure dataset consistency. This is crucial to prevent non-geological interference from the dataset, which could ultimately affect the interpretation of magnetic anomalies. In Khomutov et al. (2017), it is stated that data quality control in geomagnetic research is essential to ensure the quality of the research data before it is further processed.

3.5 Diurnal Correction

The correction is made due to deviations in the intensity of the Earth's magnetic field due to differences in measurement time and external influences such as the effects of sunlight throughout the day. These disturbances are incorporated into the measured geomagnetic data. Diurnal correction ΔH_d is calculated based on measurement results at the baseline station using the formula (Salmatia et al., 2026; Ratu et al., 2025; Sariani et al., 2024):

$$\Delta H_d = \left(\frac{t_n - t_o}{t_e - t_o}\right)(H_e - H_o) \quad (1)$$

where H_e and H_o are the magnetic field intensities at the end and initial of measurement points, respectively; t_e and t_o are the time to take the measurement at the end and initial of measurement points, respectively; and t_n is the time to take the measurement at the n-th point. The magnetic field is said to be diurnally corrected when the total magnetic field (TMI) is subtracted by ΔH_d.

3.6 IGRF Correction and Total Magnetic Anomaly

To eliminate the influence of the earth's main magnetic field which is interfered in the geomagnetic data resulting from field measurements, the magnetic field which has been diurnally corrected is substracted by the the International Geomagnetic Reference Field (IGRF). The IGRF value of the research location was obtained through the NOAA website, which is a geomagnetic reference model (NOAA, 2026). The total magnetic anomaly (TMA) is calculated using the following formula (Alawiyah et al., 2022):

$$\Delta H_{TMA} = H_{TMI} \pm \Delta H_d - H_{IGRF} \quad (2)$$

where ΔH_{TMA} and H_{TMI} are the TMA and TMI, respectively; and H_{IGRF} is the IGRF value at the study site.

3.7 Upward Continuation

Upward Continuation is used to separate regional magnetic anomaly from total magnetic anomaly (TMA) by projecting the total magnetic anomaly to a higher elevation level where the influence of local residual magnetic anomaly (LMA) is eliminated or further reduced. In other words, this transformation reduces or minimizes the influence of shallow magnetic sources near the surface while maintaining the response of deeper regional sources (Lasheen et al., 2025; Harikrishnan et al., 2023; Okoro et al., 2021). The result of this process is the regional magnetic anomaly (RMA). The Upward Continuation operator is formulated as (Okoro et al., 2021):

$$U(x, y, h) = \frac{h}{2\pi}\iint \frac{hU(x', y', 0)}{\left[(x-x')^2 + (y-y')^2 + (z-z')^2\right]^{3/2}} dx'\, dy' \quad (3)$$

where $U(x,y,h)$ is the TMA (ΔH_{TMA}) at elevation h, $U(x',y',0)$ is the TMA at the observation surface, and h is the elevation level. Upward Continuation was performed several times, raising the elevation level to 1,700 m. At this elevation, the RMA is considered separated from the TMA. This is indicated by stable or unchanged contour closures.

3.8 Residual Magnetic Anomaly

Residual or local magnetic anomaly (LMA) is a magnetic field anomaly that represents local variations due to the presence of shallow magnetic sources in the subsurface (Abdelrady et al., 2023; Sehah et al., 2020). In geomagnetic survey, LMA was obtained by subtracting TMA from RMA in the frequency domain as expressed as follows (Karim et al., 2026):

$$\Delta H_{LMA} = \Delta H_{TMA} - \Delta H_{RMA} \quad (4)$$

The residual anomaly highlights magnetic responses related to lithological contrasts and alteration zones structurally controlled by fault zones (Leão-Santos et al., 2022; El-Qassas et al., 2022). Sometimes, the presence of low magnetic anomaly zones is found to be associated with the presence of sediments in the zones (Mohammed et al., 2019).

3.9 Reduction to the Pole (RTP)

Reduction to the Pole (RTP) is a transformation used to place the residual magnetic anomaly spatially above the geological source that caused it (Stewart, 2019; Zahra and Oweis, 2019), and it is hoped that the dipolar magnetic anomaly can be transformed into a monopolar anomaly (Ghazalaa et al., 2018), thereby facilitating interpretation. This transformation was applied to residual anomaly that have undergone previous corrections. Mathematically, the RTP operator is expressed as (Stewart, 2019):

$$\mathrm{RTP}(\theta) = \frac{1}{\left[\sin(I) + i\cos(I)\cos(D-\theta)\right]^2} \quad (5)$$

where θ indicates the direction of the wave number, I and D represent the magnetic inclination and declination angles, respectively. Site magnetic inclination and declination angles of −24.79° and 0.39°, respectively, were used in this research.

3.10 Euler Deconvolution Method

Euler deconvolution (ED) method was used to estimate the lateral position and depth of magnetic anomaly sources in the subsurface based on the Euler homogeneity equation (Abraham et al., 2025; Ghanbarifar et al., 2024a; Ghanbarifar et al., 2024b; Pham et al., 2024), especially regarding the presence of lithological contact and geological structure such as fault. Euler deconvolution equation is expressed as (Ghanbarifar et al., 2024b; Pham et al., 2024):

$$(x - x_o)\frac{\partial H_{TMI}}{\partial x} + (y - y_o)\frac{\partial H_{TMI}}{\partial y} + (z - z_o)\frac{\partial H_{TMI}}{\partial z} = N(\Delta H_{RMA} - H_{TMI}) \quad (6)$$

where (x_0,y_0,z_0) are the coordinates of the anomaly source, H_{TMI} is the TMI, ΔH_{RMA} is the RMA, and N is the structural index. In this study, a Structural Index of N=0 was applied to determine the existence of lithological contact or fault zone that control the geothermal system in the Tahi Ite manifestation area. The parameter N characterizes magnetic anomaly source models, and different N values represent each specific anomaly source model as mentioned in Hosseini et al. (2025), Gamisel-Muzás et al. (2025), Ghanbarifar et al. (2024), Reid and Thurston (2014), and subsequent studies.

3.11 Second Vertical Derivative (SVD) Method

The SVD method was applied to sharpen shallow magnetic anomaly features (Yusuf et al., 2022; Alhassan et al., 2021; Obiora et al., 2018), which is useful for delineating lithological contact and fault zone (Okpoli et al., 2022; Ming et al., 2021) in the manifestation area. The SVD is derived from Laplace's potential field equation for both the gravity and magnetic fields, spatially emphasizing high-frequency components associated

with near-surface structures. The formula is (Abdelrady et al., 2024; Sumintadireja et al., 2018):

$$\frac{\partial^2 \Delta H}{\partial z^2} = -\left(\frac{\partial^2 \Delta H}{\partial x^2} + \frac{\partial^2 \Delta H}{\partial y^2} \right) \quad (7)$$

The SVD technique acts as a high-pass filter (Daoud et al., 2025), sharpening magnetic anomaly gradients, thereby clarifying the presence of structures that control geothermal system in the subsurface.

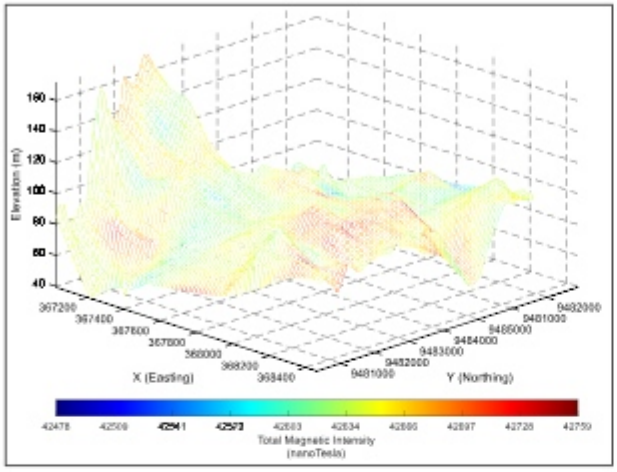

Fig 2. 3D distribution of TMI in the Tahi Ite village geothermal manifestation area.

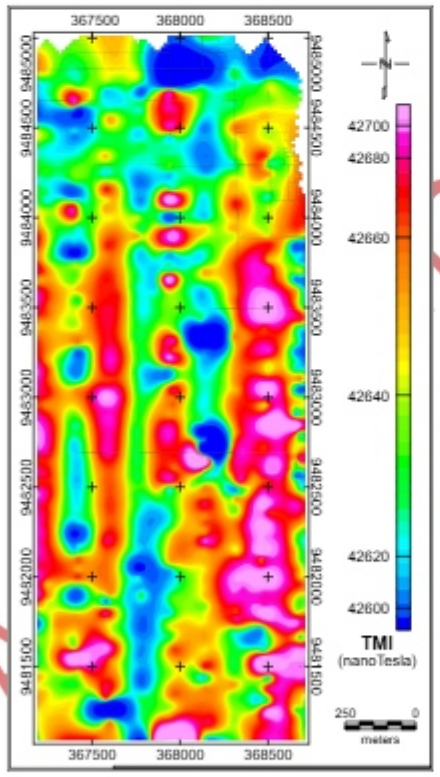

Fig 3. Contour map of TMI.

4. Results and Discussion

4.1 Total Magnetic Intensity (TMI) Distribution Patterns and Spatial Characteristics

Based on the results of data acquisition in the field, it is known that the Total Magnetic Intensity (TMI) in the Tahi Ite village geothermal manifestation area was in the range of 42,375.605 to 42,817.045 nT. The range of values of 441.44 nT illustrates the differences in the magnetic properties of subsurface rocks that are thought to be related to hydrothermal activity, the presence of lithological contacts, and geological structures such as faults in the geothermal area. In 3D, the measurement data can be observed in Figure 2, while the spatial distribution of TMI values as a contour map can be seen in Figure 3 at a scale of 1:15,000. It can be seen that the TMI pattern shows lateral variations that are not correlated with the topographic surface elevation of the measurement location. This is as can be seen in the figure, in addition to being seen at high elevation locations, high and low TMI are also seen at low elevation locations. In general, relatively low magnetic values are found in the central part of the study area, whereas higher magnetic values dominate the surrounding areas.

4.2 Corrections and Total Magnetic Anomaly (TMA) Characteristics

After data processing using diurnal and IGRF corrections, the total magnetic field anomaly (TMA) values range from approximately –137 nT to 200 nT, spatially shown in Figure 4. Diurnal variations over the four day measurement period are shown in Figure 5, which shows a trend of increasing daily fluctuations in the Earth's magnetic field from morning to afternoon and decreasing from afternoon to evening.

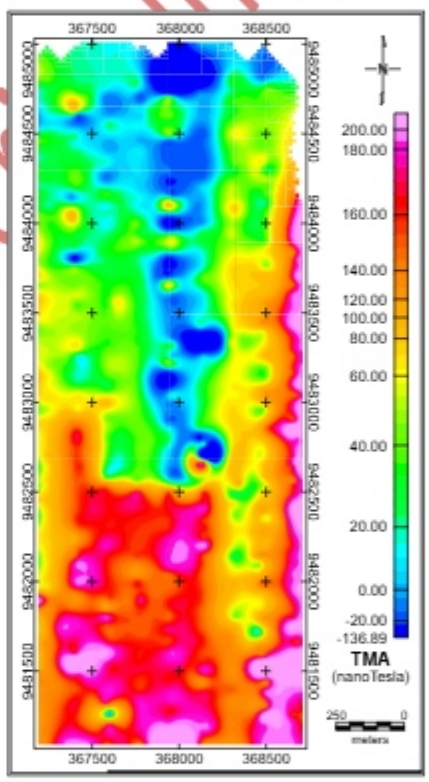

Fig 4. Contour map of TMA.

Figure 4 demonstrates quite contrasting anomaly variations. The northern and western parts of the study area are dominated by low magnetic anomaly values, indicated by blue to green colors. These locations are thought to be associated with rocks with low magnetic susceptibility or those undergoing hydrothermal alteration, which are common around geothermal systems. In the central part, a strong anomaly gradient is observed between low and high values, indicating lithological changes or the presence of geological structures such as faults that control geothermal fluid movement. Meanwhile, higher anomaly values are found in the eastern and southern parts, indicated by yellow to pink colors, indicating the presence of more magnetic rocks. The contrasting anomaly values extending or continuing from north to south confirms the presence of a fault or fracture zone oriented in the same

direction. Overall, the magnetic anomaly pattern in Tahi Ite Village indicates strong structural control over the local geothermal system. The gradient pattern and distribution of low-high anomaly zones indicate that subsurface faults act as primary permeability pathways, allowing thermal conduction or migration of hot fluids to reach the surface.

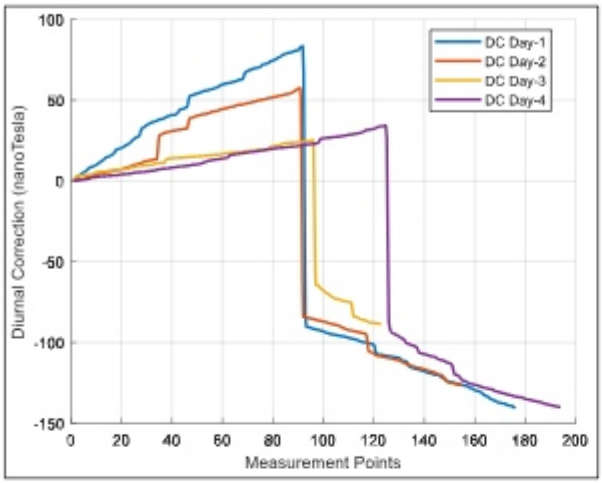

Fig 5. Diurnal correction (DC) values for each measurement point during the four day measurement period.

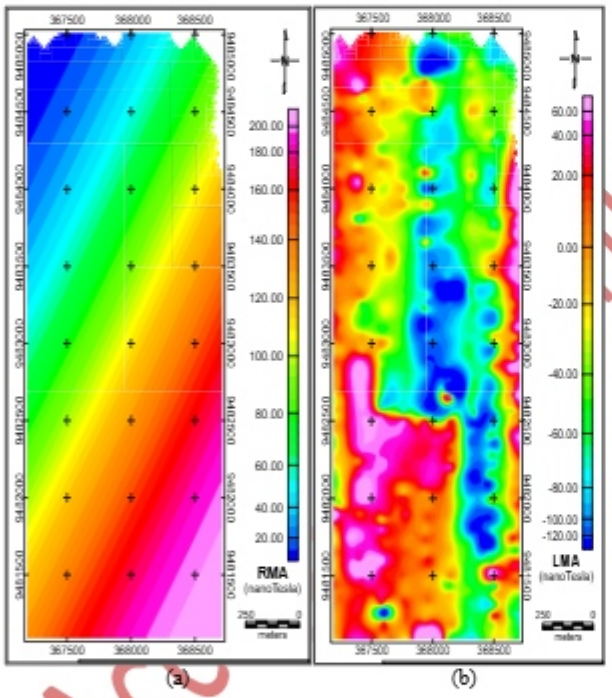

Fig 6. Contour map of magnetic anomalies in the Tahi Ite geothermal area: (a) RMA and (b) LMA.

4.3 Regional Magnetic Anomaly Derived from Upward Continuation and Estimating Residual Anomaly

Upward Continuation was applied to total magnetic anomaly (TMA) to separate regional magnetic anomaly (RMA) from total magnetic anomaly (TMA). RMA represents anomalies caused by magnetic sources located far below the surface. The continuation process is carried out through 6 height levels that are performed separately and consecutively until a representative height level is obtained, namely at heights of 200 m, 300 m, 500 m, 800 m, 1,200 m, and 1,700 m. Each elevation to each height level spatially suppresses the influence of shallow or near-surface magnetic anomaly sources. The RMA resulting from this Upward Continuation process is shown in Figure 6a, which shows a continuous and smooth contour pattern. Meanwhile, regional magnetic anomaly (LMA) is obtained by subtracting TMA from RMA, and the results can be observed in Figure 6b.

LMA is associated with shallow sources located near the surface and tend to be local in nature. The magnetic anomaly values for the Tahi Ite village geothermal area, as shown in Figure 6b, range from approximately -120 to 60 nT. Figure 6b shows that low magnetic anomalies dominate the study area in the central part with a north-south direction, and are thought to be hydrothermal alteration zones associated with the migration of geothermal fluids to the surface controlled by the presence of minor faults locally. Meanwhile, relatively high magnetic anomalies are located in the western and southeastern parts of the study area, and are likely related to lithology that is susceptible to magnetic fields. The systematic change from high to low anomalies reflects variations in shallow lithology and the intensity of hydrothermal alteration in the study area.

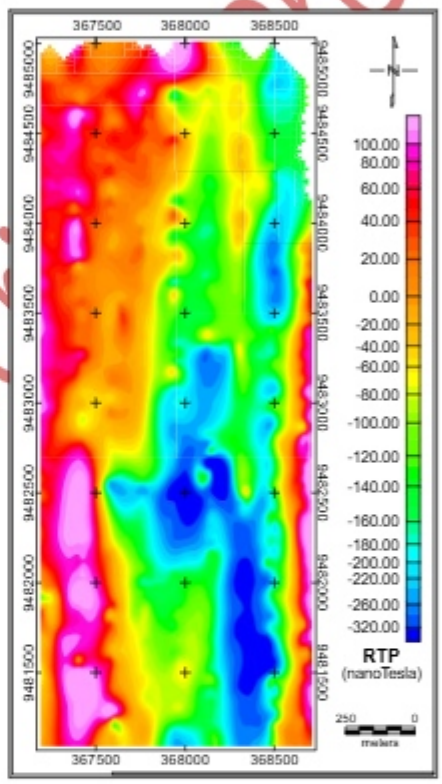

Fig 7. Contour map of RTP result on LMA in the Tahi Ite Village geothermal area.

4.4 Reduction to the Pole (RTP) Results

The residual magnetic anomaly (LMA) obtained was then subjected to Pole Reduction (RTP) to improve the accuracy of determining the lateral position of the anomaly source and facilitate interpretation. In performing this transformation process, the magnetic inclination and declination values of the study location were used, which were -24.79° and 0.39°, respectively. These values were determined using the Magnetic Field Calculators (NOAA, 2026). The RTP results in Figure 7 spatially show a more symmetrical and centralized magnetic response contour with a value range of approximately -320 to 100 nT. The RTP results indicate the presence of low magnetic anomalies that vary and extend north-south in the central part of the study area, coinciding with the location of geothermal manifestations on the surface. This spatial correspondence supports the interpretation that the low anomaly zone represents rocks that have undergone hydrothermal alteration related to thermal conduction and geothermal fluid activity to the surface.

4.5 Euler Deconvolution Results and Structural Controls on Tahi Ite Geothermal Area

Euler deconvolution (DE) was applied to the LMA that had undergone RTP, and produced a series of Euler solutions in the form of estimates of the lateral position and depth of the magnetic anomaly source. Based on the Euler deconvolution results in Figure 8a for the N=0 Structural Index, several locations of anomaly sources were identified, which are suspected to be geological contacts or faults indicated by the distribution of Euler points in blue, green, and light green. Clusters of Euler points that are arranged in a linear or continuous manner are interpreted as fault structures. In the study area, the Euler solutions indicate that there are spatially about five to eight minor faults with varying depths. The depth of the faults in the study area is grouped into four clusters as shown in Table 1, ranging from the Very Shallow zone or <15 meters to the Deep zone with a depth of >55 meters. The DE results overlaid with the residual anomaly (LMA) contour map are shown in Figure 8b, demonstrating the conformity of the Euler solution distribution with the spatial color change boundaries.

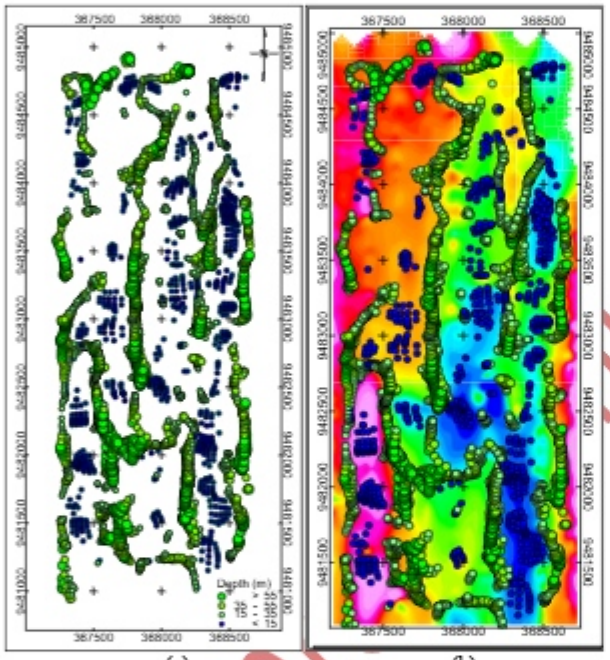

Fig 8. (a) Euler Deconvolution results for N=0 Structural Index, and (b) overlay of the Euler solutions on LMA contour map.

The continuous and segmented anomaly distribution pattern as seen in Figure 8b indicates the existence of magnetic contrast boundaries due to changes in the physical properties of rocks that commonly form along fault zones. In the Tahi Ite geothermal system, faults not only act as structures that delimit rock blocks, but are also followed by the development of minor faults as branches or secondary fractures. The presence of a continuous cluster of Euler points indicates the existence of faults that have undergone hydrothermal alteration, resulting in magnetic contrasts recorded by geomagnetic method. The termination, offset, and repeated segmentation patterns in the Euler results reflect the typical geometry of discontinuous faults that often develop as en-echelon segments. Tectonic activity, especially the activity of the main faults located approximately 2.12 km and 5.36 km from the geothermal manifestation in Tahi Ite Village, is thought to control the formation of secondary faults in the study area. Thus, the overall configuration of the Euler results indicates that linear structures in the form of faults are the main pathways for thermal conduction and hot fluid migration in the geothermal system from the reservoir to the earth's surface or in other words, which regulate the dynamics of the hydrothermal system in the geothermal area of Tahi Ite Village. Figure 9 exhibits that one of the faults intersect the Tahi Ite hot spring manifestation, while several other faults are relatively close to the hot spring manifestation.

Table 1. Grouping of Euler depth estimates into four clusters.

No.	Depth (m)	Description
1	< 15	Very Shallow
2	15 - 35	Shallow - Intermediate
3	35 - 55	Intermediate - Deep
4	> 55	Deep

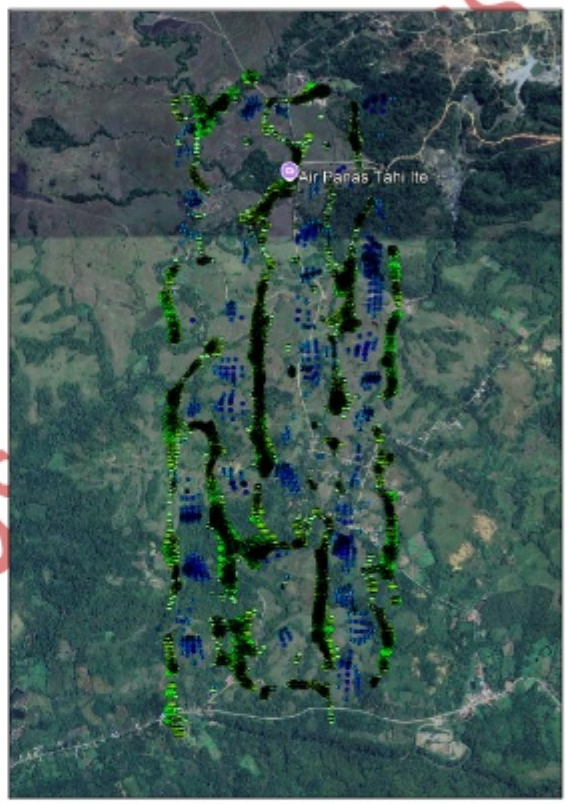

Fig 9. Overlay of the Euler deconvolution results on the Google Earth Pro imagery of the study area.

4.6 SVD Method and Structural Confirmation

The SVD method is spatially used to improve the resolution of shallow anomalies, sharpen the boundaries of lithologic contacts, and to increase the reliability of the structural patterns of minor faults identified by the previous use of the Euler deconvolution method in Figure 8. Figure 10 is an SVD map showing sharp gradient changes and alternating positive-negative anomaly patterns on the map corresponding to lithological contacts and minor fault zones. In the study area, it is estimated that there are approximately six to nine minor faults visible in the figure. As with the Euler Deconvolution results, the SVD results also exhibit that there are one or two minor faults that pass through the geothermal manifestation of Tahi Ite Village and several other faults are located relatively close to the manifestation (Figure 11). These faults likely control the geothermal system at the study area as a path for thermal conduction and migration of hot fluids. The spatial correspondence between the SVD lines and the Euler solution clusters provides strong confidence in the interpretation results regarding the existence of minor faults at the study site.

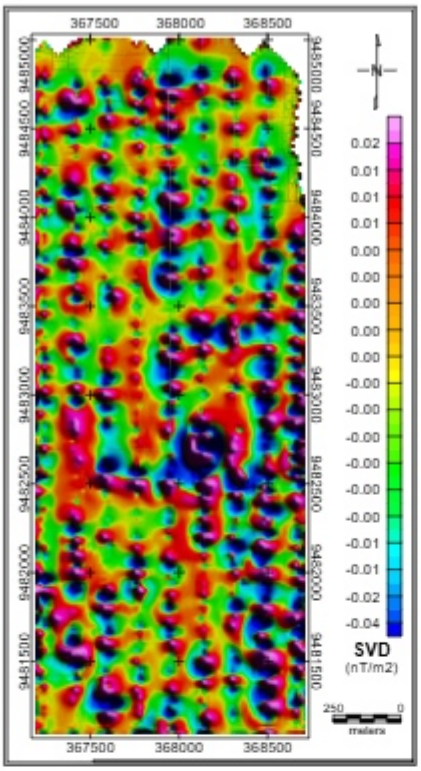

Fig 10. SVD contour map of LMA.

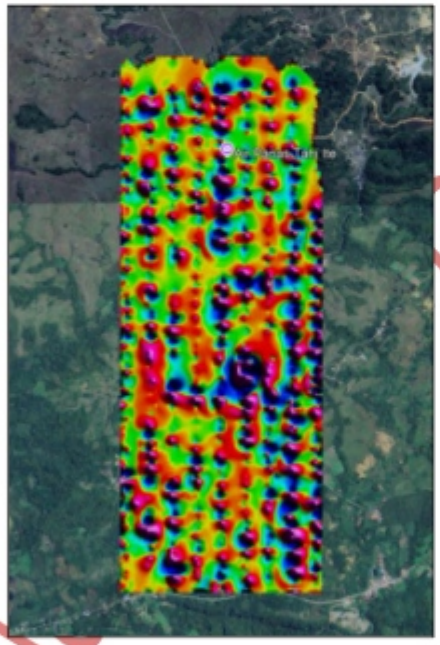

Fig 11. Overlay of SVD contour map on the Google Earth Pro imagery of the study area.

4.7 Structural Interpretation Results, Outcrops, and Geological Validation

The structural interpretation results obtained from the Euler Deconvolution method for the N=0 Structural Index and the SVD technique are supported by the geological reality observed in the field. This is evidenced by the presence of outcrops that reveal minor faults, as shown in Figure 12. The presence of outcrops that reveal minor faults at the study site serves as additional geological evidence that substantially strengthens the interpretations and findings in this study. These faults act as thermal conduction pathways and geothermal fluids to migrate from depth to the surface. Therefore, the Tahi Ite geothermal system is non-volcanic in nature and is structurally controlled by faults. In addition, this finding is in accordance with the regional geological framework of Southeast Sulawesi. This interpretation is supported by the regional geological framework of Southeast Sulawesi, which describes and provides confidence in the structural influence of the fault system in controlling geothermal manifestations at the study area. The agreement between the research results obtained geophysically, observations and realities in the field, and regional geology strengthens the reliability of the results of this study.

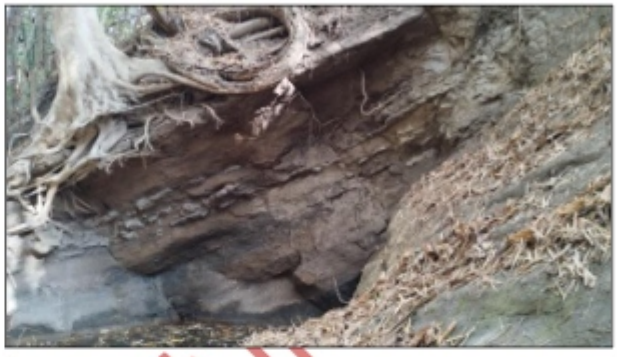

Fig 12. Rock outcrops exposed at the study area.

5. Conclusion

This study demonstrates the effectiveness of the approach using the Euler deconvolution (DE) and Second Vertical Derivative (SVD) methods in identifying subsurface structures in the geothermal manifestation area of Tahi Ite Village, Bombana Regency, Southeast Sulawesi. The results of the study show that the Total Magnetic Intensity (TMI) in the study area ranges from 42,375.605 to 42,817.045 nT. The range of values of 441.44 nT indicates variations in the magnetic properties of subsurface rocks, the presence of lithological contacts, and the influence of geological structures such as faults. The use of the DE method for the N=0 Structural Index and the SVD method on geomagnetic data successfully identified the existence of a number of minor faults in the geothermal area of Tahi Ite Village. These minor faults were classified into four clusters based on depth, namely faults located in the Very Shallow zone with a depth of <15 m, faults located in the Shallow-Intermediate zone with a depth of 15-35 m, faults located in the Intermediate-Deep zone with a depth of 35-55 m, and faults located in the Deep zone with a depth of >55 m. Based on the interpretation results, it is estimated that there are around five to nine minor faults, with around one to two of them located directly in the geothermal manifestation zone at the Tahi Ite hot spring. These minor faults are secondary structures that were likely generated by the activity of the main faults located at a distance of approximately 2.12 km and 5.36 km from the Tahi Ite hot spring, and are thought to be thermal conduction pathways and hydrothermal fluid migration to the surface. The strong spatial similarity between the Euler solution and the SVD lines in identifying and revealing the the presence of faults laterally, and the presence of a number of geological outcrops at the research site that visually reveal the presence of minor faults, provide an illustration that the interpreted structural model has strong validation and can be accounted for. Overall, the results of the study show that the Tahi Ite geothermal system is a non-volcanic geothermal system that is structurally controlled by the presence of minor faults in the area.

Acknowledgements

The authors would like to express their sincere gratitude to the Research and Community Service Institute (LPPM) of IAIN

Kendari for the research funding provided through the SBK (Litapdimas) Research Grant, Basic Research Capacity Building Cluster, Fiscal Year 2025, under Grant No. In.23/PPK/SPK/VII/00327/2025. The authors also thank the students of the Department of Geophysical Engineering, Universitas Halu Oleo, for their assistance during field data acquisition.

References

Abdelrady, M., Moneim, M.A., Alarifi, S.S., Abdelrady, A., Othman, A., Mohammed, M.A.A., Mohamed, A., 2023. Geophysical investigations for the identification of subsurface features influencing mineralization zones. Journal of King Saud University - Science, 35(7). 102809.

Abdelrady, M., Pham, L.T., Mohamed, A., Alarifi, S.S., Duong, V.H., Mohammed, M.A.A., 2024. Application of the new edge filters of aeromagnetic data to detect the subsurface structural elements controlling the mineralization in the Barramiya area, eastern desert of Egypt. Journal of King Saud University - Science, 36(11), 1-11.

Abraham, E., Usman, A., Ikeazota, I., 2025. Magnetic anomaly analysis reveals mineral potential in the Udi region of south-eastern Nigeria. Jordan Journal of Earth and Environmental Sciences, 16(3), 298-305.

Akyol, M., 2022. The relationship between urbanization, energy consumption and carbon emission. Planlama, 33(3), 421-431.

Alawiyah, S., Kadir, W.G.A., Santoso, D., Wahyudi, E.J., Aji, W., Gunawan, I., 2022. Modeling of subsurface structure by using magnetic methods in the area of Mt. Pandan, Indonesia. Arab J Geosci, 15, 1330.

Alhassan, A., Aliyu, A., Abdulhameed, Y., Bala, N., Hussaini, A., 2021, Comparison between second vertical derivative and tilt angle methods in detecting edges of gravity anomaly. IRE Journals, 5(6), 83-87.

Aljubran, M.J., Horne, R.N., 2024. Power supply characterization of baseload and flexible enhanced geothermal systems. Sci Rep, 14, 17619.

Alpine, F., Yatini, Y., Takodama, I., 2022. Identification of geothermal system in "Diana" area, Indonesia based on magnetotelluric data modelling. Journal of Geoscience, Engineering, Environment, and Technology (JGEET), 7(1), 7-14.

Anuar, M.N.A., Arifin, M.H., Baioumy, H., Nawawi M., 2021. A geochemical comparison between volcanic and non-volcanic hot springs from east Malaysia: Implications for their origin and geothermometry. Journal of Asian Earth Sciences, 221, 104938.

Castellano, J.C.A., Lacan, P., Monroy, V.H.G., García, J.A., Cortés, J.G., Audemard, F.A.M, Mancilla, O.L., Bandy, W., 2021. Geophysical characterization of a potentially active fault in the Agua Fría micro-graben, Los Azufres, Mexico. Bol. Soc. Geol. Mex, 73(2), 1-24.

Chen, H., Zheng, F., Song, R., Zhang, C., Dong, B., Zhang, J., Zhang, Y., Wu, T., 2024. Geothermal resource assessment and development recommendations for the Huangliu formation in the central depression of the Yinggehai basin. Sustainability, 16(16), 7104.

Daoud, A.M.A., Shebl, A., Abdelkader, M.M., Mohieldain, A.A., Csámer, A., Satti, A.M.N., Rózsa, P., 2025. Remote sensing and gravity investigations for barite detection in neoproterozoic rocks in the Ariab area, Red Sea hills, Sudan. Remote Sensing Applications: Society and Environment, 37, 101416.

Dashti, A., Korzani, M.G., 2021. Study of geothermal energy potential as a green source of energy with a look at energy consumption in Iran. Geothermal Energy, 9(28), 1-16.

El-Qassas, R.A.Y., 2023. Abu-Donia, A.M., Omar, A.E.A., 2023. Delineation of hydrothermal alteration zones associated with mineral deposits, using remote sensing and airborne geophysics data. A case study: El-Bakriya area, central eastern Desert, Egypt. Acta Geodaetica et Geophysica, 58, 71-107.

Gamisel-Muzás, A., Soto, R., Ayala, C., Mochales, T., Rubio, F.M., Clariana, P., Rey-Moral, C., Martín-León, J., 2025. The geological structures of the pyrenees and their peripheral basins examined through EMAG2v2 magnetic data. Solid Earth, 16, 251-274.

Ghanbarifar, S., Hosseini, S.H., Abedi, M., Afshar, A., 2024a. A dynamic window-based Euler depth estimation algorithm for potential field geophysical data. Bollettino di Geofisica Teorica ed Applicata, 65(3), 399-438.

Ghanbarifar, S., Hosseini, S.H., Ghiasi, S.M., Abedi, M., Afshar, A., 2024b. Joint Euler deconvolution for depth estimation of potential field magnetic and gravity data. International Journal of Mining and Geo-Engineering, 58(2), 121-134.

Gutiérrez-Negrín, L.C.A., 2024. Evolution of worldwide geothermal power 2020-2023. Geothermal Energy, 12(14), 1-60.

Harikrishnan, P.R., Lasitha, S., Suseel, A.S., Twinkle, D., 2023. Tectonic significance of the shear zones in Southern Granulite Terrane: An integrated geophysical study. Geosystems and Geoenvironment, 2(2), 100151.

Hermawan, D., Sugianto, A., Yushantarti, A., Munandar, A., and Widodo, S., 2011. Kajian Panas Bumi Non-Vulkanik Daerah Sulawesi Bagian Tenggara. Bandung: Pusat Sumber Daya Geologi, Badan Geologi, KESDM.

Hosseini, S.H., Afshar, A., Abedi, M., Ganbarifar, S., Oskooi, B., Moradi, S., 2025. Fixed window joint Euler deconvolution for depth estimation of magnetic and gravity data in the Shavaz region. Sci Rep., 15(1), 42054.

https://www.esdm.go.id/

https://www.iagi.or.id/

Huang, J., Abed, A.M., Eldin, S.M., Aryanfar, Y., Alcaraz, J.L.G., 2023. Exergy analyses and optimization of a single flash geothermal power plant combined with a trans-critical CO_2 cycle using genetic algorithm and Nelder-Mead simplex method. Geothermal Energy, 11(4), 1-20.

IRENA (International Renewable Energy Agency) and IGA (International Geothermal Association), 2023. Global geothermal market and technology assessment. https://www.irena.org/publications/2023/Feb/Global-geothermal-market-and-technology-assessment

Jamil, F., Shafiq, I., Sarwer, A., Ahmad, M., Akhter, P., Inayat, A., Shafique, S., Park, Y.K., Hussain, M., 2023. A critical review on the effective utilization of geothermal energy. Energy & Environment, 35(1), 438-457.

Karim, A., Tripathi, A., Low, U., Ansari, M.T., Yadav, D., Prasad, K.N., 2026. Identification of structurally controlled potential mineralization zones in Chhotanagpur Gneissic Complex, Eastern India from gravity and magnetic data. Geosystems and Geoenvironment, 5(2), 100470.

Khomutov, S.Y., Mandrikova, O.V., Budilova, E.A., Arora, K., Manjula, L., 2017. Noise in raw data from magnetic observatories. Geosci. Instrum. Method. Data Syst., 6, 329-343.

Kusnadi, D., 2021. Laporan Akhir Survei Rinci Geokimia (Pertagastech) Daerah Panas Bumi Nage Kabupaten Ngada, Provinsi Nusa Tenggara Timur. Bandung: Pusat Sumber Daya Mineral, Batubara dan Panas Bumi, Badan

Geologi, KESDM.
Lasheen, E.S.R., El-Badry, B.A., Mohamed, W.H., Khouqeer, G.A., Sanislav, I.V, Sami, M., 2025. Radioactivity and aeromagnetic of magmatic suites, Arabian nubian shield: Petrological and health risk characteristics. Journal of Radiation Research and Applied Sciences, 18(4). 101910.
Leão-Santos, M., Moraes, R., Li, Y., Raposo, M.I., Zuo, B., 2022. Hydrothermal alteration zones, magnetic susceptibility footprints and 3D model of iron oxide-copper-gold (IOCG) mineralization, Carajás Mineral Province, Brazil. Minerals, 12(12), 1581.
Manyoe, I.N., Hutagalung, R., 2020. Subsurface shallow modelling based on resistivity data in the hot springs area of Libungo geothermal, Gorontalo, Indonesia. Journal of Geoscience, Engineering, Environment, and Technology (JGEET), 5(2), 75-80.
Manzella, A., 2017. Geothermal energy. EPJ Web of Conferences, 148, 1-26.
Massinai, M.A., Mulyadi, D., Hendrajaya, L., Abdullah, C.I., Nurhasanah, N., Setiawan, A., 2026. Unveiling geothermal potential in Pinrang regency, Indonesia. Geothermics, 122, 103107.
Ming, Y., Ma, G., Li, L., Han, J., Wang, T., 2021. The spatial different order derivative method of gravity and magnetic anomalies for source distribution inversion. Remote Sensing, 13(5), 964.
Mohammed, A., Adewumi, T., Kazeem, S.A., Abdulwaheed, R., Adetona, A.A., Usman, A., 2019. Assessment of geothermal potentials in some parts of upper benue trough northeast Nigeria using aeromagnetic data. Journal of Geoscience, Engineering, Environment, and Technology (JGEET), 04(01), 7-15.
NOAA, 2026. https://www.ngdc.noaa.gov/geomag/calculators/magcalc.shtml?model=igrf
Obiora, D.N., Idike, J.I., Oha, A.I., Soronnadi-Ononiwu, C.G., Okwesili, N.A., Ossai, M.N., 2018. Investigation of magnetic anomalies of Abakaliki area, southeastern Nigeria, using high resolution aeromagnetic data. J. Environ. Eng. Geophys., 10(6), 57-71.
Okoro, E.M., Onuoha, K.M., Okeugo, C.G., Dim, C.I.P., 2021. Structural interpretation of High-resolution aeromagnetic data over the Dahomey basin, Nigeria: implications for hydrocarbon prospectivity. J Petrol Explor Prod Technol, 11, 1545-1558.
Okpoli, C.C., Ogbole, J.O., Victor, O.A., Okanlawon, G.O., 2022. Mineral exploration of Iwo-Apomu Southwestern Nigeria using aeromagnetic and remote sensing. The Egyptian Journal of Remote Sensing and Space Science, 25(2), 371-385.
Pandarinath, K., Shankar, R., Santoyo, E., Shetty, S.B., García-Soto, A.Y., Gonzalez-Partida, E., 2019. A rock magnetic fingerprint of hydrothermal alteration in volcanic rocks: An example from the Los Azufres geothermal field, Mexico. Journal of South American Earth Sciences, 91, 260-271.
Pandarinath, K., González-Partida, E., Santoyo, E., Ramos-Leal, J.A., 2023. Hydrothermal alteration of surficial rocks at Los Humeros geothermal field, Mexico: a magnetic susceptibility approach. Arabian Journal of Geosciences, 16, 262.
Pham, L.T., Oliveira, S.P., Abdelrahman, K., Gomez-Ortiz, K., Nguyen, D.V., Vo, Q.T., Eldosouky, A.M., 2024. Selection of Euler deconvolution solutions using the enhanced horizontal gradient and stable vertical differentiation. Open Geosciences, 16(1), 20220637.
Ratu, M.D., Manan, A., Bahdad, and Chahyani, R., 2025. Identification of subsurface structure using the pseudo-gravity method of magnetic data at the geothermal area of Sonai village and its surroundings, Puriala, Konawe Regency. Indonesian Physics Communication, 22(2), 73-84.
Reid, A.B., Thurston, J.B., 2014. The structural index in gravity and magnetic interpretation: errors, uses, and abuses. Geophysics, 79(4), J61-J66.
Ricks, W., Voller, K., Galban, G., Norbeck, J.H., Jenkins, J.D., 2025. The role of flexible geothermal power in decarbonized electricity systems. Nature Energy, 10, 28-40.
Risdianto, D., Permana, L.A., Wibowo, A.E.A., Sugianto, A., Hermawan, D., 2015. Sistem Panas Bumi Non-Vulkanik di Sulawesi. Bandung: Pusat Sumber Daya Mineral, Batubara dan Panas Bumi, Badan Geologi, KESDM.
Saepuloh, A., Ramadhan, S.F., Riawan, E., Abdillah, M.R., Gumilar, I., Iskandar, I., 2026. Revealing mechanism of phreatic eruptions derived by satellite and field based water interactions at Tangkuban Parahu volcano, west Java, Indonesia. Journal of Volcanology and Geothermal Research, 471, 108528.
Salmatia, W., Manan, A., Bahdad, Chahyani, R., Andimbara, L., 2026. Application of SVD method using magnetic data to identify subsurface structures at the geothermal area of Sonai village and its surroundings, Puriala, Konawe. Jurnal Ekologi, Masyarakat dan Sains, 6(2), 215-224.
Sariani, Manan, A., Bahdad, Chahyani, R., 2024. Estimation of subsurface structure using Euler deconvolution method of magnetic data at the geothermal area of Sonai village and its surroundings, Konawe regency. JURNAL GEOCELEBES, 8(2), 162-177.
Sehah, Raharjo, S.A., Risyad, A., 2020. A geophysical survey with magnetic method for interpretation of iron ore deposits in the eastern Nusawungu coastal, Cilacap regency, central Java, Indonesia. Journal of Geoscience, Engineering, Environment, and Technology (JGEET), 5(1), 37-44.
Simandjuntak, T.O., Surono, Sukido, H., 1993. Peta Geologi Lembar Kolaka Skala 1:250.000. Bandung: Pusat Penelitian dan Pengembangan Geologi, KESDM.
Stewart, I.C.F., 2019. A simple approximation for low-latitude magnetic reduction-to-the-pole. Journal of Applied Geophysics, 166, 57-67.
Stober, I., Bucher, K., 2021. Geothermal Energy: From Theoretical Models to Exploration and Development, 2nd Ed. Cham: Springer Nature Switzerland AG.
Sumintadireja, P., Dahrin, D., Grandis, H., 2018. A Note on the use of the second vertical derivative (SVD) of gravity data with reference to Indonesian cases. J. Eng. Technol. Sci., 50(1), 127-139.
Surono, 2013. Geologi Lengan Tenggara Sulawesi. Bandung: Badan Geologi, KESDM. https://geologi.esdm.go.id/storage/publikasi/JE7ZurXikq6pjMxA4fsi0BDAnQiSqZLNPqUIW4HK.pdf
Taufan, Y.A., Syafri, I., Nur, A.A., Risdianto, D., Zarkasyi, A., Rahadinata, T., Awaludin, W., 2020. Resistivity models of Pantar island geothermal system, East Nusa Tenggara, Indonesia. Journal of Geoscience, Engineering, Environment, and Technology (JGEET), 5(3), 113-118.
Thilakarathna, M.P., Abeysinghe, A.M., Subasinghe, N.D., 2025. Use of ground magnetic survey in exploration of geothermal springs in a metamorphic terrain: A case study from Sri Lanka. Geothermics, 133, 103486.
Titus, K., Archer, R., Peer, R., Dempsey, D., 2023. Carbon negative geothermal: Theoretical efficiency and sequestration potential of geothermal-BECCS energy

cycles. International Journal of Greenhouse Gas Control, 122, 103813.
Yan, X., Xin, B., Cheng, C., Han, Z., 2024. Unpacking energy consumption in China's urbanization: Industry development, population growth, and spatial expansion. Research in International Business and Finance, 70(A), 102342.
Yusuf, S.N., Imagbe, L.O., Yohanna, O.M., Ibrahim, Y., Kuku, A.Y., 2022. Imaging magmatic intrusions using derivatives of high-resolution aeromagnetic data over the Nigerian sector of the chad basin. Scientific African, 16, e01211.
Zahra, H.S., Oweis, H.T., 2019. Application of high-pass filtering techniques on gravity and magnetic data of the Eastern Qattara Depression area, Western Desert, Egypt. NRIAG Journal of Astronomy and Geophysics, 5(1), 106-123.